AD_____

Award Number: DAMD17-03-1-0257

TITLE: Nanoparticle-mediated rescue of p53 through targeted degradation of mdm2

PRINCIPAL INVESTIGATOR: Nicholas O. Fischer, OTHD

CONTRACTING ORGANIZATION: University of Massachusetts
                          Amherst, MA 01003

REPORT DATE: September 2006

TYPE OF REPORT: Annual Summary

PREPARED FOR: U.S. Army Medical Research and Materiel Command
               Fort Detrick, Maryland 21702-5012

DISTRIBUTION STATEMENT: Approved for Public Release;
                        Distribution Unlimited

The views, opinions and/or findings contained in this report are those of the author(s) and should not be construed as an official Department of the Army position, policy or decision unless so designated by other documentation.

REPORT DOCUMENTATION PAGE

1. REPORT DATE *(DD-MM-YYYY)* 01-09-2006	2. REPORT TYPE Annual Summary	3. DATES COVERED *(From - To)* 18 Aug 2003 – 17 Aug 2006

4. TITLE AND SUBTITLE	5a. CONTRACT NUMBER
Nanoparticle-Mediated Rescueof p53 through Degradation of MDM2	5b. GRANT NUMBER DAMD17-03-1-0257
	5c. PROGRAM ELEMENT NUMBER

6. AUTHOR(S)	5d. PROJECT NUMBER
Nicholas O. Fischer, OTHD	5e. TASK NUMBER
E-Mail: fischer29@llnl.gov	5f. WORK UNIT NUMBER

7. PERFORMING ORGANIZATION NAME(S) AND ADDRESS(ES)	8. PERFORMING ORGANIZATION REPORT NUMBER
University of Massachusetts Amherst, MA 01003	

9. SPONSORING / MONITORING AGENCY NAME(S) AND ADDRESS(ES)	10. SPONSOR/MONITOR'S ACRONYM(S)
U.S. Army Medical Research and Materiel Command Fort Detrick, Maryland 21702-5012	11. SPONSOR/MONITOR'S REPORT NUMBER(S)

12. DISTRIBUTION / AVAILABILITY STATEMENT
Approved for Public Release; Distribution Unlimited

13. SUPPLEMENTARY NOTES
Original contains color plates: All DTIC reproductions will be in black and white

14. ABSTRACT

The interaction between MDM2 and p53 is a viable therapeutic target, as overexpression of MDM2 can lead to excessive p53 degradation, suppressing a cell's ability to cope with cellular insult. The goal of this research is to use recent advances in nanotechnology to develop a specific nanoparticle antagonist to disrupt the MDM2:p53 interaction. Inhibiting the interaction between p53 and MDM2 allows wild-type p53 concentrations to rise to functional levels, effectively killing proliferating tumor cells. By incorporating traditional peptide inhibitors of MDM2 with mixed-monolayer protected gold cluster nanoparticles, we hope to effect MDM2 denaturation on the nanoparticle surface, increase peptide stability, and facilitate intracellular peptide delivery. Nanoparticle characteristics, such as size, surface chemistry and biocompatibility, may be controlled and modified for these specific applications. Our findings demonstrated that nanoparticles decorated with inhibitory peptides can be used to inhibit the MDM2:p53 interaction. Further optimization of the nanoparticles is required for successful implementation in therapeutic applications.

15. SUBJECT TERMS
MDM2, p53, nanoparticles, peptides

16. SECURITY CLASSIFICATION OF:			17. LIMITATION OF ABSTRACT	18. NUMBER OF PAGES	19a. NAME OF RESPONSIBLE PERSON USAMRMC
a. REPORT U	b. ABSTRACT U	c. THIS PAGE U	UU	15	19b. TELEPHONE NUMBER *(include area code)*

Table of Contents

Introduction

The interaction between MDM2 and p53 is a viable therapeutic target. Overexpression of MDM2 can lead to excessive degradation of p53, suppressing a cell's ability to cope with cellular insult.[1] MDM2-conferred tumorigenicity has been implicated in a number of human tumors, including breast cancer.[2-5] Disruption of the MDM2:p53 interaction enables functional levels of p53 to accumulate, allowing cells to either halt cell division or initiate apoptosis.[6] Numerous studies have been successful in disrupting the MDM2:p53 interaction using inhibitory peptides,[7,8] peptide analogs,[9-11] or polycyclic compounds.[12-16] These inhibitors target the deep hydrophobic cleft of MDM2 that interacts with the N-terminal α-helix of p53. Although promising, many of these approaches have inherent challenges ranging from stability in cellular environments to cellular delivery. Based on these limitations, an approach integrating specificity, stability, internalization and biocompatibility is needed. The advent of nanoparticle technology may present an ideal way to address these issues.

Our group has demonstrated the versatility of nanoparticles in biological settings, ranging from plasmid transfection of mammalian cells to tunable binding of protein surfaces.[17-20] These studies validate the biological application of nanoparticles and suggest that they can be used to inhibit MDM2. The disruption of the p53:MDM2 interaction can rescue cells that are characterized by wild type p53 and overexpressed MDM2. Nanoparticles functionalized with a previously studied p53 peptide[7] will be used to specifically bind MDM2. Upon binding, MDM2 may denature on the surface of the nanoparticle, removing the potential for release and further action on p53. Given the relative size and surface functionality, each nanoparticle will be able to bind multiple copies of MDM2. This provides an efficient means of effectively decreasing intracellular MDM2 concentrations, allowing p53 to reach wild type levels, thus enabling a cellular approach to tumor elimination.

Body
Synthesis of peptide-tagged nanoparticles

The design of a nanoparticle to specifically binding HDM2 (the human variant of MDM2) requires a number of key features. First, the unfunctionalized nanoparticle must be able to resist nonspecific binding, ensuring that any binding is due solely to the incorporated recognition element. Nanoparticles featuring a tetra(ethylene glycol) monolayer (EG4) fit this criterion. Second, the peptide recognition element must be synthesized to not only bind HDM2, but also to facilitate incorporation into the nanoparticle monolayer. This is accomplished by conjugating a thiol-capped linker to the peptide. An outline of the synthesis is described in Figure 1.[21]
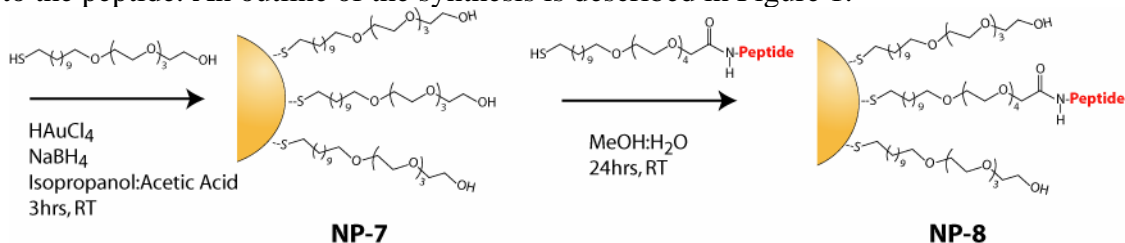

Figure 1. Synthesis of EG4-functionalized gold nanoparticles (**NP-7**), followed by incorporation of the peptide recognition unit through a place-exchange reaction (NP-8).

4

For these studies, gold nanoparticles featuring the neutral hydroxyl tetra(ethylene glycol) ligand (Ligand **3**) were synthesized (**NP-7**). Nanoparticles were synthesized directly in the presence of Ligand **3**. While the size of **NP-7** was slightly larger (3 ± 1 nm, Figure 2), the nanoparticles were completely water soluble and stable in a variety of physiologically-relevant buffers.
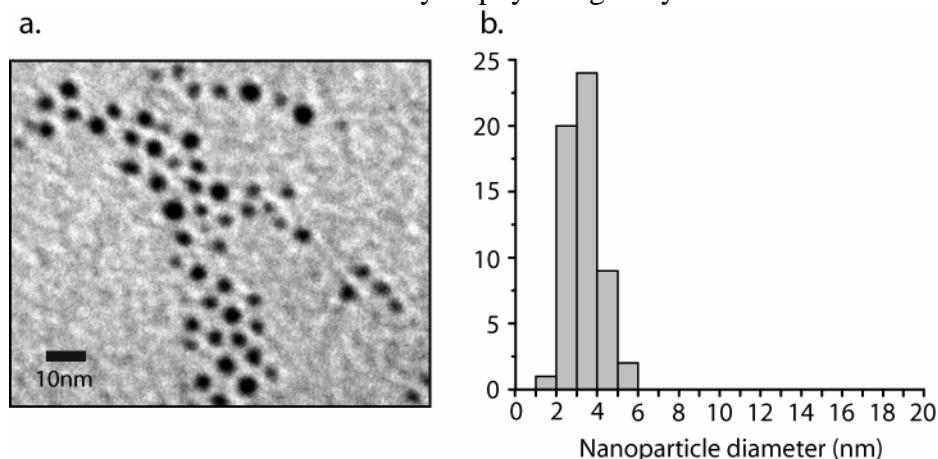

Figure 2. Transmission electron micrograph of **NP-7**. b. Histogram of **NP-7** with 3.3 ± 0.7 nm core diameters (error based on S.D.; n = 56).

A previously reported HDM2 inhibiting peptide was chosen as the recognition element (Peptide **1**: *N*-Met-Pro-Arg-Phe-Met-Asp-Try-Trp-Glu-Gly-Leu-Asn-NH$_2$).[7] Although this peptide was not the most potent derivative designed by Garcia-Echeverria and coworkers, it is comprised solely of natural amino acids and has a 28-fold greater affinity to HDM2 than the native p53 sequence. The peptide was synthesized by solid phase peptide synthesis using standard Fmoc chemistry. To facilitate subsequent incorporation into the nanoparticle monolayer, Ligand **4** was conjugated to the N-terminus of the peptide by diisopropylcarbodiimide (DIC) coupling. The acetylated peptide was also synthesized as a control for subsequent activity assays. Identities of the peptide and peptide-linker conjugate were verified by mass spectrometry.

Peptide **1** was successfully incorporated into the **NP-7** monolayer by a place-exchange reaction (Figure 1) to give **NP-8**. The exchange was carried out in a mixed solvent system (1:1 MeOH:H$_2$O) due to the hydrophobic nature of the Peptide **1**-linker conjugate. The nanoparticles were purified by extensive dialysis against water to remove excess ligand. **NP-8** displayed similar solubility and stability in aqueous buffer as **NP-7**. The electrophoretic mobility of the nanoparticle was tested to confirm incorporation of the peptide ligand (Figure 3a). The migration of **NP-8** towards the cathode indicates that peptide incorporation was successful, as the peptide is slightly anionic (pI = 6.7). As expected, the neutral **NP-7** showed no significant mobility. The absorbance spectra of the two nanoparticles overlap, indicating that no changes in particle size or morphology occur during the place exchange reaction (Figure 3b). This was confirmed by TEM. Interestingly, subtraction of the **NP-7** spectra from **NP-8** reveals a characteristic peptide spectrum (Figure 3b-inset). These data confirm that the peptide has been successfully incorporated into the **NP-8** monolayer. To determine the amount of peptide on the nanoparticle surface, nuclear magnetic resonance (NMR) was utilized. By comparing the signal integration of aromatic residue in the peptide with EG4, the peptide:EG4 ratio was estimated at 1:20. Assuming that the nanoparticle monolayer is comprised of 1000 ligands (based on 3 nm average size and MW of **NP-7**),[22] the number of peptides per nanoparticle was calculated at 20.
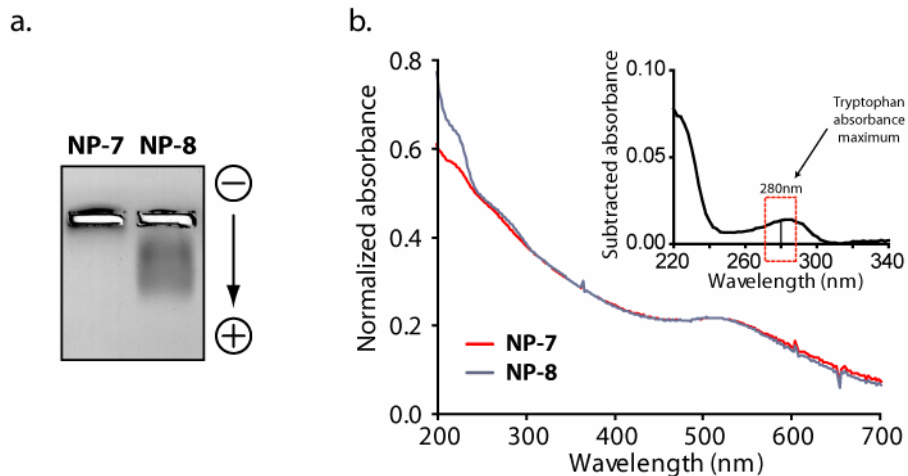
Figure 3. a. Gel mobility before and after peptide incorporation into **NP-7** monolayer. b. Absorbance spectra of **NP-7** and **NP-8**. Peptide signal of **NP-8** is revealed upon subtraction of the **NP-7** spectra (inset).

Inhibition of HDM2 by NP-8

To determine the inhibitory effects of **NP-8** on the p53-HDM2 interaction, an in vitro competition binding assay was performed (Figure 4). In this competition assay, ELISA plates were coated with p53-GST. After preincubation of purified HDM2 with different amounts of peptide, **NP-7**, and **NP-8**, the samples were added to the immobilized p53 and the fraction of HDM2 bound to p53 was detected with a series of antibodies (see Figure 4a for details). The design of this competition assay ensures that multiple copies of HDM2 can be bound by each nanoparticle. As expected, the peptide alone exhibited an IC_{50} of 252 ± 28 nM, concurrent with the cited value of 300 nM (Figure 4b).[7] Based on the peptide fraction of the nanoparticle, the IC_{50} of **NP-8** is 1420 ± 340 nM. Furthermore, **NP-7** has no detrimental effect on the p53-HDM2 interaction, indicating that the EG4 periphery of the monolayer is sufficient in preventing interactions with either HDM2 or p53 due to non-specific binding. These results are very promising, in that they clearly demonstrate that peptides tagged to the nanoparticle surface retain intrinsic activity.
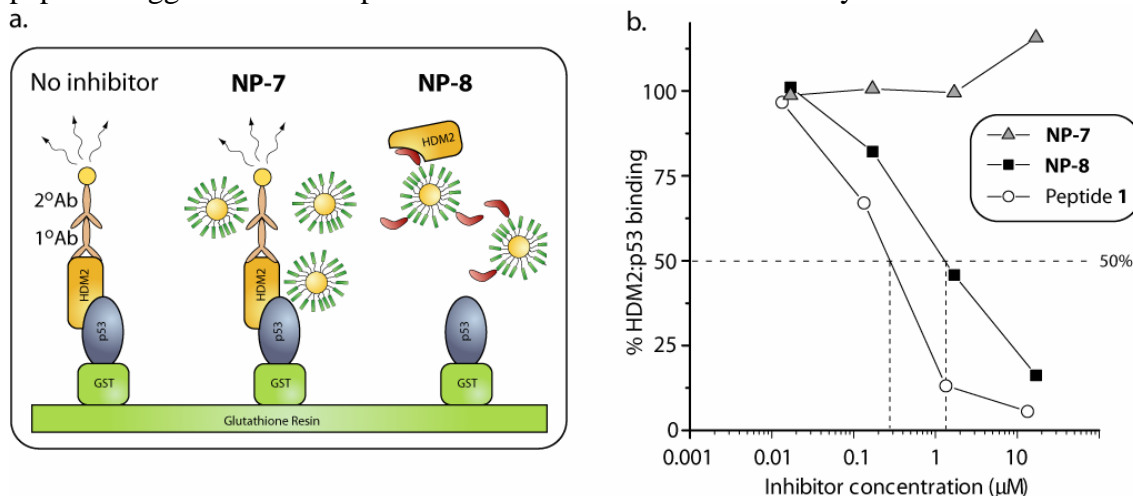

Figure 4. a. In vitro binding assay to determine inhibition of the p53-HDM2 protein-protein interaction. b. Results of the assay indicated that **NP-8** significantly inhibits HDM2, while unfunctionalized **NP-7** does not.

Optimization of peptide ligand and nanoparticle base

While preliminary results demonstrate the effective inhibition of the HDM2:p53 interaction by peptide-decorated nanoparticles, the initial inhibitor design presented some obstacles that needed to be addressed. Chief among these are: 1) determination of the peptide concentration on the nanoparticle surface to allow direct comparisons of inhibition by NP-peptide and free peptide, 2)

adequate nanoparticle purification to avoid erroneous inhibition profiles by unincorporated peptide ligands, and 3) increasing the spacing between peptide and nanoparticle surface to ensure a spatially favorable presentation of the peptide. To address these issues, modifications in the design of the peptide, the thiol linker, and the nanoparticle were required.

Peptide and thiol linker optimization

Peptide solubility is an important factor in nanoparticle purification and accurate determination of peptide concentration. If completely water soluble, the peptide ligand can be separated from the peptide-nanoparticle conjugate by either centrifugation or dialysis, and, by determining peptide concentration in the centrifugation supernatants and washes, the amount of unincorporated can be quantified. This allows a more accurate estimation of the degree of peptide incorporation into the nanoparticle monolayer than NMR integration. Peptide **1**, while itself soluble in aqueous solution, has four hydrophobic and three aromatic residues. Upon conjugation to the thiol linker (Ligand **4**), the combination of hydrophobic residues on the peptide and hydrophobic alkane chain of the linker render the ligand insoluble in water. Recently, hydrophilic derivative of the p53-based peptide were developed by Zhang and coworkers (Peptide **2**: Phe-Lys-Lys-Ac$_6$c-Trp-Glu-Glu-Leu).[23] This peptide is designed for cofacial presentation of the key residues (Phe[19], Trp[23], Leu[26]) by incorporating features to enhance water solubility and α-helix formation. These include two pairs of Lys (*i*) and Glu (*i* + 4) to promote intrahelical electrostatic interactions and the incorporation of the helix promoter 1-amino-1-cyclohexane carboxylic acid (Ac$_6$c) immediately prior to the Trp residue. To further increase the hydrophilicity of the peptide, and to address the distance between peptide and monolayer, an extra EG3 spacer was incorporated between the thiol linker and the N-terminus of the peptide (Figure 5a).
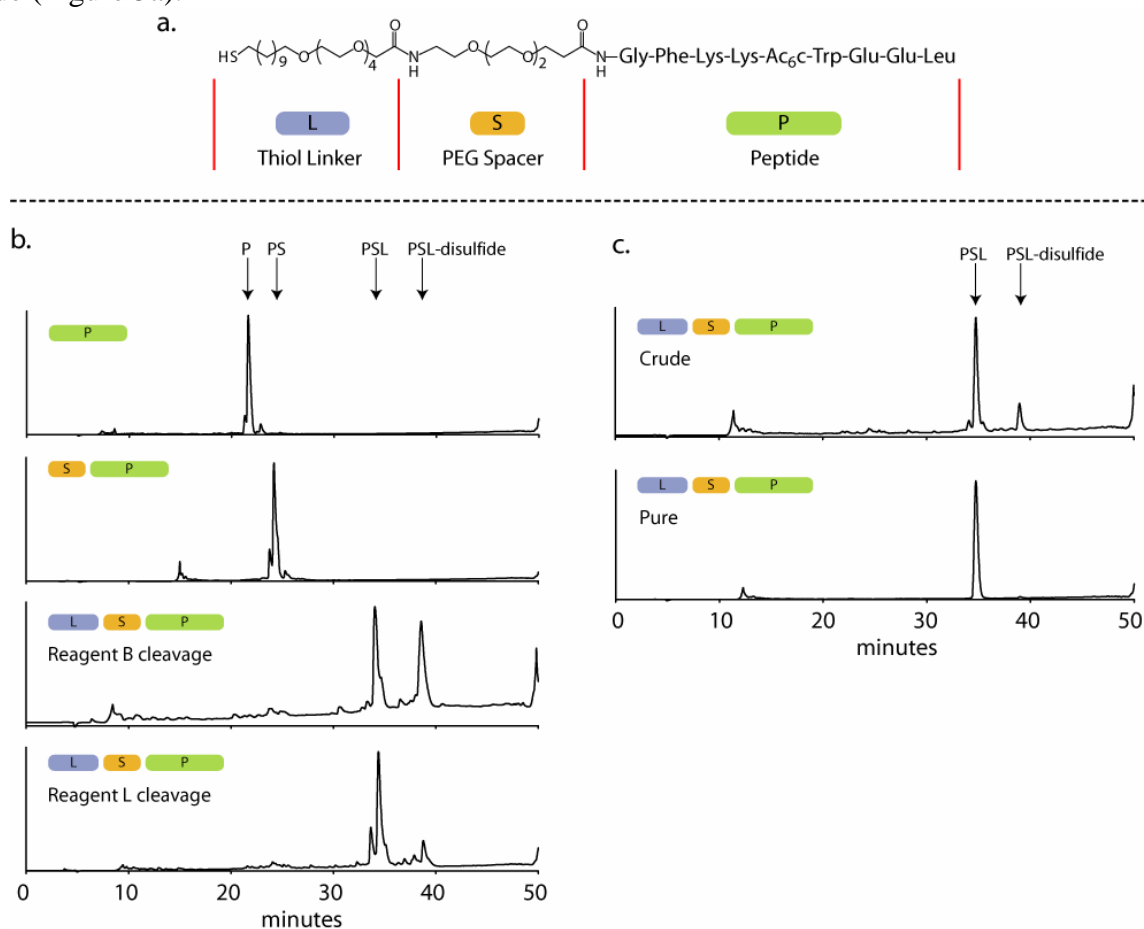

Figure 5. a. Design of the tripartite Peptide **2** ligand for nanoparticle conjugation, composed of Ligand **4**, a novel PEG spacer, and the hydrophilic Peptide **2**. b. Analytical HPLC analysis of conjugation product. Resin cleavage/deprotection

cocktails lacking reducing agents resulted in significant disulfide formation. c. Analysis of final product before and after preparatory HPLC. All HPLC chromatograms represent absorbance at 220 nm.

Peptide **2** was synthesized manually by solid phase peptide synthesis to enable conjugation of the appropriate linker moieties. Standard Fmoc chemistry was used to generate Peptide **2**. An additional glycine residue was inserted at the N-terminus to increase the spacing between the active peptide segment and the linker moieties. The EG3 spacer was designed as an amino acid derivative, facilitating conjugation to the peptide. However, extensive double-coupling using diisopropylcarbodiimide (DIC) was required for complete conjugation. Ligand **4** was conjugated in a similar manner. Each step in the synthesis was monitored by analytical HPLC to ensure completion of the reaction. As seen in Figure 5b, definitive shifts in elution times were observed as each successive moiety was conjugated. Unfortunately, this peptide-linker conjugate was sensitive to oxidation, as significant disulfide formation was observed using a cleavage cocktail lacking a reducing agent, resulting in peptide dimers (as determined by mass spectrometry). Reduction of this disulfide was achieved post-cleavage using tris(2-carboxyethyl)phosphine hydrochloride (TCEP), although reduction was incomplete. This suggests that a certain degree of segregation may take place between the hydrophilic peptide segment and the hydrophobic linker, facilitating the formation of disulfides between closely packed peptide chains. The inefficient reduction of these disulfides by TCEP may be due to the very hydrophobic microenvironment of the disulfide bond, minimized access of the hydrophilic reducing agent. However, a majority of the disulfides can be prevented from forming initially by using a cleavage cocktail containing dithiothreitol (DTT), as demonstrated in Figure 5.9b. Final purification was achieved using preparative HPLC, resulting in a product that was greater than 90% pure (Figure 5c). Acetylated Peptide **2**, lacking the thiol linker and PEG spacer, was also purified to greater than 95% purity. A comparison of inhibitory potential demonstrates that Peptide **2** has a higher IC_{50} than Peptide 1 (0.7 µM vs. 0.3 µM, respectively, see Figure 6).
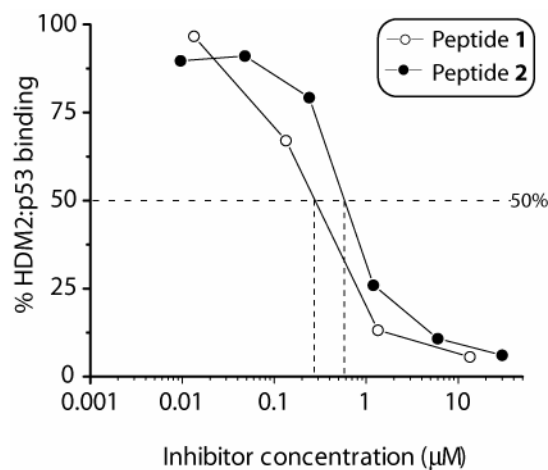

Figure 6. Comparison of HDM2 inhibition by Peptide **1** and Peptide **2**.

NP-7 was successfully decorated with the Peptide **2** ligand. Ligand exchange reactions were conducted overnight in water, providing water soluble nanoparticle-peptide conjugates. Nanoparticles could be loaded with varying amounts of peptide, as demonstrated by subsequent electrophoretic mobility shift assays (Figure 7). As each reaction constituent was water soluble, purification was conducted by centrifugation. Due to the small size of precursor **NP-7** particles (3 nm ± 1 nm), ultracentrifugation at 200,000g for 1 hour was required for proper sedimentation. While analysis of the peptide concentrations retained in the wash supernatants afforded approximate quantification of incorporated peptide, residual nanoparticle contaminants in these washes precluded more precise quantification. Due to the polydisperse size range found in the preparation of the **NP-7**

nanoparticles, centrifugation may not consistently pellet those particles below 1 nm in size. To address this obstacle, nanoparticles featuring larger gold cores were investigated.
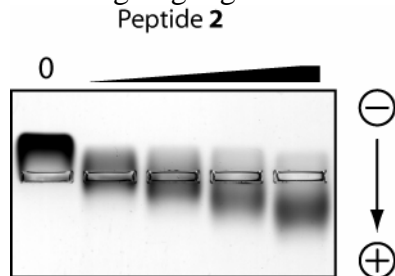

Figure 7. Electrophoretic mobility of nanoparticles is dependent on the degree of peptide incorporation. Peptide-nanoparticle conjugates migrate to the cathode due to the slight anionic nature of the peptide (pI ≈ 6.5).

Nanoparticle optimization

To investigate the utility of nanoparticles featuring larger gold cores, citrate-stabilized nanoparticles were synthesized. These particles, due to their larger size, can be easily centrifuged at 13,000 rpm for 30 minutes to form a loose pellet. The synthesis involves the nucleation of gold atoms in the presence of excess sodium citrate. The concentration of citrate dictates the ultimate size of the particle, and citrate functions as a capping ligand on the gold surface. For our application, the synthetic approach of Grabar and coworkers was used to generate nanoparticles with core diameters of ca.13 nm (**NP-9**, Figure 8a).[24] Compared to the **NP-7** derivatives previously used, the large nanoparticles are significantly more monodisperse in size (Figure 8b).
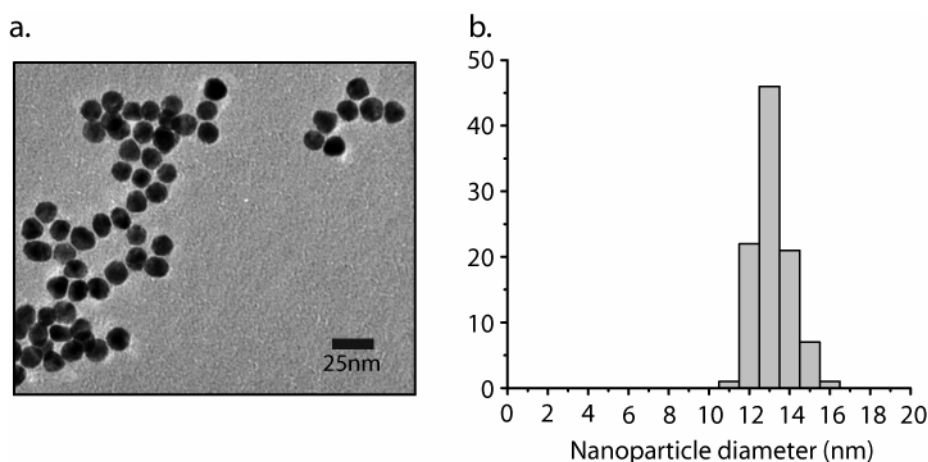

Figure 8. a. Transmission electron micrograph of citrate-stabilized gold nanoparticle, **NP-9**. b. Histogram of **NP-9** with 13.1 ± 0.9 nm core diameters (error based on S.D.; n = 98).

Nanoparticles of larger size (core diameters >3nm) have very distinct absorbance profiles, characterized by a surface plasmon band. The position and width of this band can be correlated to size and size distribution of the nanoparticle. Also, a shift or broadening of the surface plasmon band indicates a change in core size, perhaps due to particle agglomeration. In the case of 13 nm **NP-9**, the peak absorbance of this band is at 518, as demonstrated in Figure 5.13a (black trace). The citrate-stabilized nanoparticles exhibit limited stability in buffered aqueous solutions. This is due to the weak, yet extensive, interactions between the gold surface atoms and citrate. To afford greater stability, as well as biocompatibility, the nanoparticles were exchanged with Ligand **3**, featuring the neutral tetra(ethylene glycol) moiety (**NP-10**). A number of studies have highlighted the difficulty of functionalizing these particles, as displacement of the citrate leads to rapid aggregation of the gold cores.[25,26] However, the EG4 component of Ligand **3** appears to mitigate any interparticle interactions during the exchange, as no agglomeration is observed in the presence of excess ligand. The absorbance spectrum of **NP-10** exhibits only a slight shift in the plasmon band to 520 nm,

without significant broadening (Figure 9a, red trace). The increased stability of **NP-10** is demonstrated upon addition of salt (Figure 9b). While the citrate-stabilized nanoparticles readily aggregate and precipitate at very low salt concentrations, indicated by a red shift and broadening of the surface plasmon band, the particles functionalized with Ligand **3** are stable even at salt concentrations exceeding 1 M. These nanoparticles can be tailored to incorporate charged functionality on the monolayer periphery, either through subsequent place exchange reactions, or by initial exchange of the citrate-stabilized nanoparticles with mixed ligands (Figure 9c). As seen in Figure 9d, **NP-10** (Lane 1) can be completely exchanged with anionic Ligand **4** (lane 2). Mixed monolayers exchanged with 10% Ligand **4** or Ligand **5** can also be achieved (lanes 3 and 4, respectively). These data demonstrate that larger gold core nanoparticles can be readily synthesized and functionalized in an identical manner as our smaller particles.
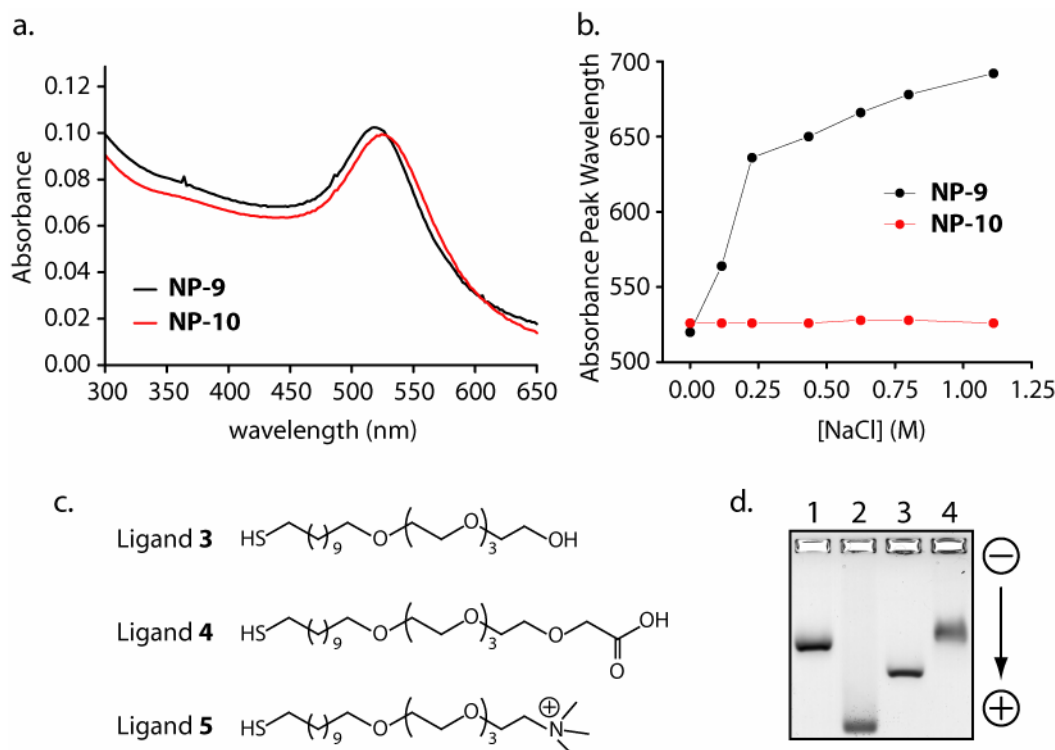

Figure 9. a. Absorbance spectra of citrate-stabilized nanoparticle before and after exchange with Ligand **3** (black and red traces, respectively). b. Salt-induced shifts in plasmon band are observed only with **NP-9** not exchanged with Ligand **3**. c. Ligands used for place exchange onto **NP-10** for charge incorporation. d. Gel electrophoresis of **NP-10** derivatives (1, **NP-10**; 2, **NP-10** (100% Ligand **4**); 3, **NP-10** (10% Ligand **4**); 4, **NP-10** (10% Ligand **5**)).

Inhibition of HDM2 by NP-11

Two strategies were used to functionalize citrate-stabilized nanoparticles with Peptide **2** (Figure 10). The first strategy relied on the place exchange of the peptide onto the EG4-functionalized **NP-10**. Initially, citrate stabilized nanoparticles were exchanged completely with Ligand **2**. After purification, the particles were then incubated with the Peptide **2** ligand. Conversely, citrate stabilized nanoparticles were exchanged simultaneously with both Ligand **2** and Peptide **2**.
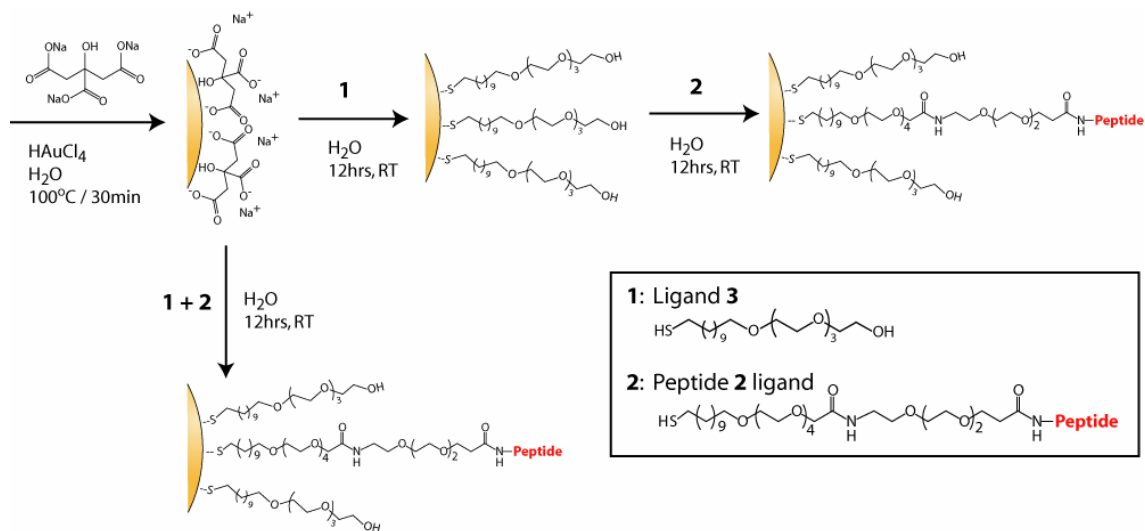
Figure 10. Incorporation of Peptide **2** ligand onto **NP-10** to give **NP-11**. All exchange reactions are carried out in water.

Each of exchange strategies was successful in incorporating peptide into the nanoparticle monolayer, generating **NP-11**. Gel mobility shift assays indicate that Peptide **2** was successfully incorporated into the **NP-11** monolayer (Figure 11a). This is demonstrated by a greater mobility towards the cathode since the peptide is slightly anionic (pI = 6.5). Absorbance spectroscopy corroborates incorporation of Peptide 2, while demonstrating that the ligand exchange reactions have no effect on the nanoparticle core size or size distribution (Figure 11b). Subtraction of the absorbance spectra delineates contribution of the peptide to the **NP-11** signal.
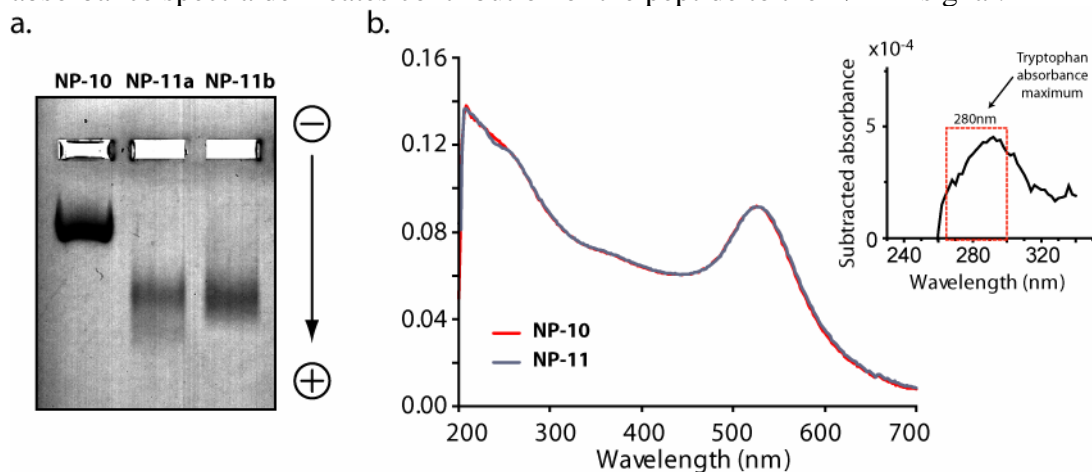

Figure 11. a. Gel mobility shift of **NP-10** and **NP-11** with two different concentration of incorporated Peptide **2** ligand. b. Absorbance spectroscopy of **NP-10** and **NP-11**. Inset of subtracted spectra shows characteristic peptide absorbance at 280 nm.

To determine the efficacy of **NP-3** on inhibiting the p53-MDM2 interaction, an ELISA was performed (Figure 12). Unfortunately, the results from the inhibition assay were less striking than with **NP-8**. Inhibition is clearly observed with **NP-11b** (functionalized with a greater degree of peptide), while little to no inhibition occurs in the presence of **NP-10** and **NP-11a**. While disappointing, it is clear that the nanoparticle-peptide conjugates are able to inhibit the p53-MDM2 interaction, albeit with lower efficiency than previously thought.
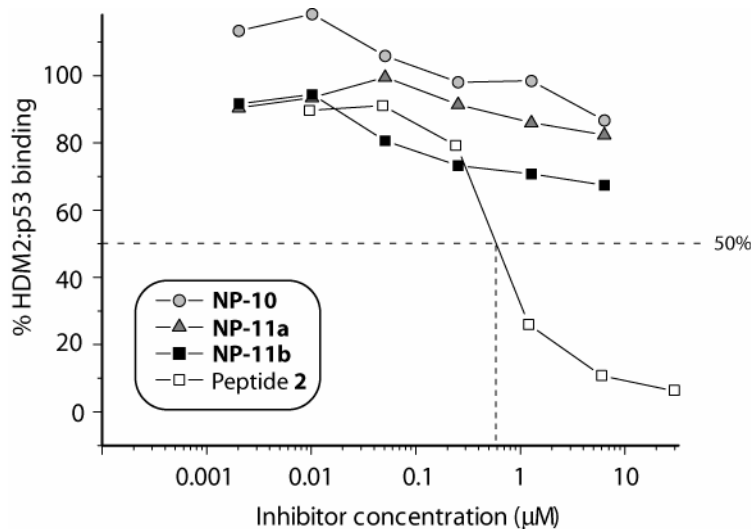
Figure 12. Inhibition of HDM2 by **NP-11** at two different peptide loadings. ELISA setup is identical as previously described.

Future Work

Although I have graduated, this work is being continued by current students of Prof. Vincent Rotello. Below is an outline of the research currently underway to fully optimize the nanoparticles and to extend their use for *in vivo* applications in cultured cells.

Optimization of the nanoparticle-peptide conjugates is required to demonstrate the benefits of peptide conjugation to nanoparticles for protein surface inhibition. Currently, a few obstacles must be overcome. 1) The nanoparticle-peptide conjugates are not completely stabile in physiological buffers. **NP-11**, for example, is currently stable only in high pH buffers, possibly due to the interparticle peptide-mediated interactions at in a lower pH range. This can be mitigated by controlling the peptide coverage on the nanoparticle. In addition, the incorporation of Peptide **1** may abrogate this pH sensitivity, since Peptide 1 does not have the electrostatic pairing potential of Peptide **2** (which is due to the Glu-Lys pairs). 2) The quantification of peptide on the nanoparticle surface remains a difficult endeavor. While the ability to easily purify both peptide and nanoparticle is helpful, the amount of peptide actually incorporated into the monolayer is very small. By increasing the amounts of nanoparticle and peptide used for the exchange reactions, it may be possible to more accurately determine incorporated peptide concentrations by UV-Vis. If not, an alternate method is required, such as tagging the peptide with a fluorophore. This would have two advantages, namely allowing quantification by fluorescence (a more sensitive technique) as well as providing a marker for cellular uptake studies using fluorescence microscopy (see Figure 13 for preliminary evidence of NP internalization). 3) The current peptides exhibit IC_{50}s in the low micromolar or high nanomolar range. To effectively demonstrate inhibition by nanoparticle-peptide conjugates, the concentration of nanoparticle required to achieve the necessary peptide concentration is very high. Increasing the peptide loading on the nanoparticle may not address this issue, as too high a loading will result in peptide crowding and spatial restriction on HDM2 binding. One way to circumvent this issue is to use a peptide with a very high binding affinity to the nanoparticle, such as the Peptide **1** derivative designed by Garcia-Echeverria and coworkers (Ac-Phe[19]-Met-Aib-Pmp-6ClTrp[23]-Glu-Ac$_3$c-Leu[26]-Asn-NH$_2$).[7] Although this peptide is rather expensive to synthesize due to the costly nonnatural amino acids incorporated into the primary sequence (α-aminoisobutyric acid (Aib), phosphonomethyl-phenylalanine (Pmp), 6-chloro-L,D-tryptophan (6ClTrp), and 1-aminocyclopropanecarboxylic acid (Ac$_3$c)), the 5 nM IC_{50} may significantly decrease the required peptide concentration for sufficient inhibition. If this peptide is used in conjunction with sparse anionic charges in the nanoparticle monolayer, inhibition is expected to be significant at low overall nanoparticle concentrations.
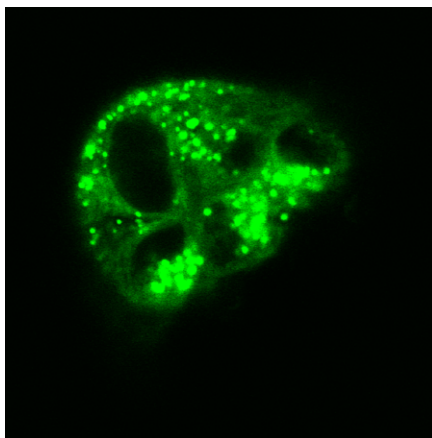
12

Figure 13. Confocal fluorescence micrograph of internalized bodipy-labeled nanoparticles in breast epithelial tumor cells (MCF-7) .

Once the nanoparticle-peptide conjugates are optimized for in vitro inhibition of the p53-HDM2 interaction, their efficacy in HDM2 inhibition *in vivo* can be studied, using two cell lines expressing different levels of HDM2. MCF-7 cells have elevated levels of HDM2 and suppressed levels of wild-type p53. As a control, T47-D cells express low levels of HDM2 but express high levels of mutant p53. The effects of nanoparticle incubation (vs. naked peptide) will be monitored in two ways: 1) determination of intracellular HDM2 and p53 levels and 2) induction of apoptosis and cell death. As particle uptake may be an issue, positively charged tranduction peptides (such as the nuclear localization signal, NLS) can be conjugated to the nanoparticle to facilitate cellular uptake. These studies should demonstrate the applicability of nanoparticle-peptide conjugates in true cellular environments.

Key Research Accomplishments

- Expression and purification of HDM2 and p53 with cleavable GST tags
- Synthesis of peptide and peptide-linker conjugate
- Synthesis of stable and water-soluble peptide-functionalized nanoparticles
- Development of hydrophilic peptide
- Optimization of peptide tether, incorporating additional ethylene glycol moieties
- Synthesis of 13 nm gold-core nanoparticles and subsequent functionalization
- Disruption of HDM2:p53 interaction
- Preliminary confocal microscopy studies of nanoparticle uptake

Training Accomplishments:

This research requires the integration of numerous areas of expertise, from synthetic chemistry to biology. The development of the nanoparticle-based inhibitors allowed me to learn the synthesis of different types of gold-core nanoparticles, including functionalization strategies to enable their use in biological environments. The design of the peptide-based ligand further expanded my knowledge in automated and manual peptide synthesis, chemical coupling strategies, and the use of analytical and preparatory HPLC. Development and optimization of the ELISA involved molecular cloning, protein expression and purification, and the systematic quantification and analysis of protein

binding. Preliminary work in nanoparticle delivery also afforded me the opportunity to work with various cultured cell types and to employ confocal microscopy for live cell imaging. Overall, working on this project has allowed me to greatly expand my technical expertise and, more importantly, to gain insight into the fundamentals of interdisciplinary research.

Reportable Outcomes

Employment:

Post-doctoral Fellow at Lawrence Livermore National Laboratory, CA

   Start Date: 10.31.2005

Successful thesis defense based on project research:

Title: Nanoparticle receptors for protein surface binding

Degree: Ph.D., Molecular and Cellular Biology Program

Presentations based on project research:

American Chemical Society National Conference (Philadelphia, PA) Aug 2004. *Nanoparticle-mediated rescue of p53 through targeted binding of MDM2.* (Accepted as poster presentation in Division of Organic Chemistry)

Gordon Research Conference: Drug Carriers in Medicine and Biology (Bozeman, MT) Sept 2004. *Nanoparticle-mediated inhibition through protein surface binding.* (Accepted as poster presentation. Could not attend due to medical emergency)

Era of Hope 2005: Department of Defense Breast Cancer Research Program Meeting (Philadephila, PA) June 2005. *Nanoparticle-mediated rescue of p53 through targeted degradation of MDM2.*

Additional post-doctoral employment offers based on project research:

U.S. Naval Research Laboratory, Division of Optical Sciences (Dr. H. Mattoussi)

Conclusions

   The overarching goal of this research was to develop nanoparticles for the selective inhibition and denaturation of HDM2 in hopes of presenting a therapeutic modality for breast cancer treatment. The preliminary research aims have been addressed with marked success, demonstrating that nanoparticles decorated with inhibitory peptides can be used to inhibit protein-protein interactions, specifically the interaction between HDM2 and p53. Although inhibition using nanoparticle-conjugated peptides is currently not as effective as naked peptides, the further functionalization of nanoparticle with small chemical functional groups or larger macromolecules may demonstrate the benefits of using monolayer protected nanoparticles for biomedical applications.

References

1. D. A. Freedman, L. Wu, A. J. Levine, *Cell Mol Life Sci* **55**, 96-107 (1999).

2. M. Cuny *et al., Cancer Res* **60**, 1077-83 (2000).

3. B. Quesnel, C. Preudhomme, J. Fournier, P. Fenaux, J. P. Peyrat, *Eur J Cancer* **30A**, 982-4 (1994).

4. A. Marchetti *et al., J Pathol* **175**, 31-8 (1995).

5. R. W. Zhang, H. Wang, *Curr Pharm Des* **6**, 393-416 (2000).

6. P. Chene, *Nature Rev. Cancer* **3**, 102 (2003).

7. Garcia-Echeverria, C., Chene, P., Blommers, M. J. & Furet, P. *J. Med. Chem.* 43, 3205–3208 (2000).

8. V. Böttger *et al.*, *Oncogene* **13**, 2141-7 (1996).

9. S. J. Duncan *et al., J. Am. Chem. Soc.* **123**, 554–560 (2001).

10. R. Fasan *et al., Angew. Chem. Intl. Ed.* **43**, 2109-2112 (2004).

11. J. A. Kritzer, J. D. Lear, M. E. Hodsdon, A. Schepartz, *J. Am. Chem. Soc.* **126**, 9468-9 (2004).

12. N. Majeux, M. Scarsi, A. Caflisch, *Proteins* **42**, 256–268 (2001).

13. J. Zhao *et al., Cancer Lett.* **183**, 69–77 (2002).

14. R. Stoll *et al., Biochemistry* **40**, 336–344 (2001).

15. P. S. Galatin, D. J. Abraham, *J. Med. Chem.* **47**, 4163-4165 (2004).

16. L. T. Vassilev *et al, Science* **303**, 844-848 (2004).

17. K. K. Sandhu, C. M. McIntosh, J. M. Simard, S. W. Smith, V. M. Rotello, *Bioconjug. Chem.* **13**, 3-6 (2002).

18. N. O. Fischer, C. M. McIntosh, J. M. Simard, V. M. Rotello, *Proc. Natl. Acad. Sci. U. S. A.* **99**, 5018-23 (2002).

19. N. O. Fischer, A. Verma, C. M. Goodman, J. M. Simard, V. M. Rotello, *J. Am. Chem. Soc.* **125**, 13387-91 (2003).

20. R. Hong, N. O. Fischer, A. Verma, C. M. Goodman, T. Emrick, V. M. Rotello, *J. Am. Chem. Soc.* **126**, 739-43 (2004).

21. A. G. Kanaras, F. S. Kamounah, K. Schaumburg, C. J. Kiely, M. Brust. *Chem. Commun.*, 2294-2295 (2002).

22. M.J. Hostetler *et al. Langmuir* **14**, 17-30 (1998).

23. R. Zhang *et al. Anal. Biochem.* **331**, 138-46 (2004).

23. N.L. Rosi, C.A. Mirkin. *Chem. Rev.* **105**, 1547-1562 (2005).

24. K.C. Grabar, R.G. Freeman, M.B. Hommer, M.J. Natan. *Anal. Chem.* **67**, 735-743 (1995).

25. C. Burda, X. Chen, R. Narayanan, M.A. El-Sayed. *Chem. Rev.* **105**, 1025-1102 (2005).

26. K. Aslan, V.H. Perez-Luna. *Langmuir* **18**, 6059-6065 (2002).